Available online at www.sciencedirect.com
ScienceDirect
Trans. Nonferrous Met. Soc. China 31(2021) 1561−1571
Transactions of Nonferrous Metals Society of China
www.tnmsc.cn

Effects of extrusion speed of continuous extrusion with double billets on welding performance of 6063 Al alloy

Ying ZHAO, Jiu-yang PEI, Li-li GUO, Xin-bing YUN, Huai-chao MA

Engineering Research Center of Continuous Extrusion, Ministry of Education, Dalian Jiaotong University, Dalian 116028, China

Received 10 June 2020; accepted 22 December 2020

Abstract: During continuous extrusion, the welds were formed at the confluence of two billets. Influences of extrusion wheel rotational speed on micromorphology and properties of welds of 6063 Al alloy were investigated through microstructure observation, tensile test, and SEM analyses. Welding parameters were analyzed using finite element simulation. Results indicated that metal welding was remarkably affected by oxide on outer surface of the double billets during continuous extrusion. Degree of oxide breakage on the welding surface increased due to the evident increase in effective strain rate with increasing extrusion speed. The high temperature induced by increased extrusion speed accelerated the formation of metallurgical bonding. A portion of weld seam lines slowly disappeared, and the proportion of the welding interface that failed to reach metallurgical bonding was also gradually reduced. Tensile strength and elongation of the weld specimen increased with the increase of extrusion speed.

Key words: continuous extrusion; 6063 Al alloy; extrusion speed; welding performance

1 Introduction

With the development of high-speed trains, high-speed ships, and other transportation equipment, the demand for aluminum alloy panels with large width has increased. The majority of panels have been extruded via horizontal extrusion in recent years [1]. Extrusion pressure is high because of the small size in thickness direction. Horizontal extrusion is a three-step process of casting→ heating→ extrusion. Continuous extrusion is a green, energy-saving, and environment-friendly processing method without heating that involves casting → continuous extrusion. Figure 1 shows the schematic diagram of continuous extrusion. Rotatable extrusion wheel consists of two grooves in its periphery. Billets are pressed into grooves under the pressure of coining roll and rotate with the extrusion wheel until abutments raised in grooves block them and then flow into the chamber through respective feeding inlets. Two billets subsequently converge and weld in the chamber. The final product with a weld seam is extruded. Large-size products are extruded through expansion forming, which easily causes uneven structure and properties of products, because billets demonstrate a smaller size in continuous extrusion than in conventional extrusion. The combination of continuous extending extrusion and weld formation of two or more billets is suitable for aluminum alloy panels with large widths. Considerably less energy consumption in continuous extrusion than in horizontal extrusion indicates its high potential for the development. However, the weld seam formed during continuous extrusion with double billets can remarkably affect the quality of the final product.

Corresponding author: Ying ZHAO, Tel: +86-411-84109397, E-mail: zhaoying@djtu.edu.cn
DOI: 10.1016/S1003-6326(21)65598-X

The weld formed during continuous extrusion of two billets is different from that formed in conventional extrusion with a porthole die. The material in conventional extrusion experiences division and welding, which occur between virgin metals, through the porthole die [2−4]. Hence, effects of oxide on the welding are minimal. By comparison, the weld during continuous extrusion with double billets is formed between billets without the division stage. Thus, the oxide on the outer surface of the billet inevitably affects the welding process. However, studies on welding characteristics in continuous extrusion with double billets are rarely reported.

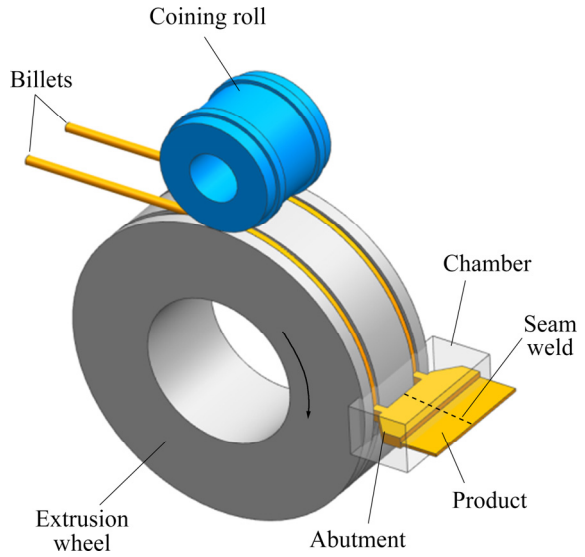

Fig. 1 Schematic diagram of continuous extrusion

Extrusion speed is a complex parameter for welding. Many researchers have investigated effects of extrusion speed on weld seam through numerical simulations and experiments. LIU et al [5] revealed that the welding pressure, effective stress, and temperature are related to welding increase with the increase in extrusion speed. LIU et al [6] investigated effects of extrusion speed on the weld quality of magnesium alloys and demonstrated that the increase in welding pressure and product temperature due to the increase in extrusion speed are the main causes of improved weld strength. YU et al [7] showed that the increase in extrusion speed contributes to the formation of new grains and closure of micro-voids during welding. However, LI et al [8] argued that the extrusion at high extrusion speeds can lead to poor welding quality of the product. BAI et al [9] offered that welding time is also important to welding quality of the product and bonding strength increases with the decrease in extrusion speed. However, the influences of continuous extrusion speed on the welding have not been reported.

Therefore, the effects of continuous extrusion speed on the weld quality were investigated in this study. Extrusion speed was changed by altering the extrusion wheel rotational speed. The welding quality was analyzed through microstructure observation, tensile test, and SEM analyses. The characteristics of welding stress, effective stress, welding temperature, and effective strain rate related to the welding were evaluated through finite element method (FEM).

2 Experimental

Commercial 6063 aluminum alloy was adopted in this study. Diameters of billets and the extrusion wheel are 9.5 and 350 mm, respectively. This study applied the following extrusion process: billet clearing → continuous extrusion → water quenching → artificial aging treatment. Billet surfaces were cleaned with alcohol to eliminate impurities. The billets and the extrusion wheel were used at room temperature, while dies and chamber were preheated to 450 °C before extrusion. The product was quenched via on-line water cooling after extrusion and then artificial aging treatment was applied at 200 °C for 2 h.

Experiments were conducted to analyze weld seams of the 6063 aluminum alloy under various extrusion wheel rotational speeds (n) of 6, 7, 9, and 11 r/min. Figure 2(a) shows the cross-section of the 80 mm-wide and 6 mm-thick extruded product. Length, width, and thickness directions of the product are denoted by LD, WD, and TD, respectively. Observation specimens of welding, transition and matrix zones, denoted by A, B, and C on the cross-section, respectively, were obtained from extruded products. An aqueous solution of 50% hydrofluoric acid was used as the etchant for metallographical observation.

Figure 2(b) shows the positions of tensile specimens. Matrix specimens were cut parallel to the weld line, and weld seam specimens were cut at 90° and 45° to the weld line via wire electro discharge machining. Figure 2(c) presents

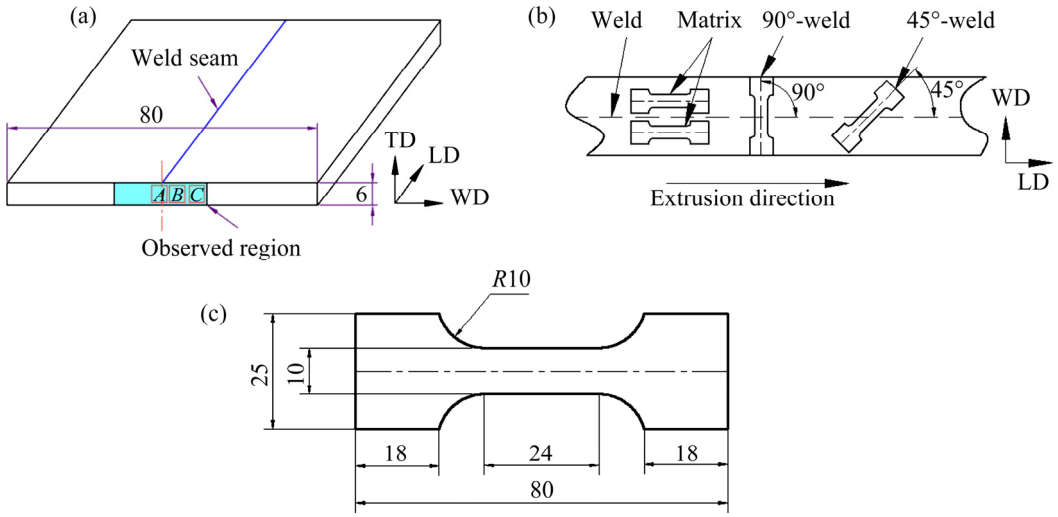

Fig. 2 Positions and dimensions of tensile specimens: (a) Cross-section of product; (b) Positions of specimens; (c) Dimensions of specimens (unit: mm)

the dimension details of tensile specimens. Fracture surfaces and the composition were observed and analyzed via SEM. The temperature at the outlet of the product was measured with an infrared thermometer (Marathon MM 3M). Emissivity was set to 0.2. Resistance strain sensor was placed behind the abutments to test the stress.

3 FE model

Continuous extrusion was simulated by DEFORM-3D software. Only half of the geometry was built because the model is symmetrical (Fig. 3). The diameter and length of billet were 9.5 and 1600 mm, respectively. A thermo-viscoplastic material model of the 6063 aluminum alloy was used for the billet, and a thermo-rigid material model of AISI H13 was utilized for the extrusion wheel, coining roll, dies, and chamber. A shear friction model was adopted for the friction between the billet and tools. The friction coefficient at the interface between the billet and extrusion wheel was set to be 0.95 to represent a nearly sticking condition. Table 1 shows the material properties and simulation parameters. Flow stress of 6063 aluminum alloy as a function of strain, strain rate and temperature is illustrated in Fig. 4.

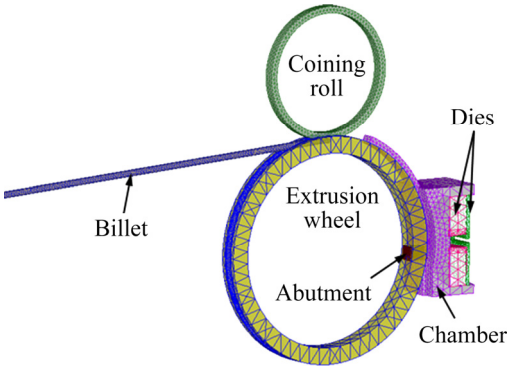

Fig. 3 Finite element model of continuous extrusion of 6063 aluminum alloy

Table 1 Material properties and simulation parameter

Material property	Value	Simulation parameter	Value
Material	AA6063	Billet diameter/mm	9.5
Heat capacity/ ($J\cdot kg^{-1}\cdot K^{-1}$)	901	Extrusion wheel diameter/mm	350
Thermal conductivity/ ($W\cdot m^{-1}\cdot K^{-1}$)	180.3	Initial billet temperature/°C	20
		Initial die temperature/°C	450
Friction coefficient	0.95 (wheel), 0.4 (other tools)	Rotational speed of extrusion wheel/ ($r\cdot min^{-1}$)	6, 7, 9, 11

4 Results

4.1 Microstructure

Figures 5−7 display the metallographic cross-section microstructures through the welding region at different extrusion wheel rotational speeds. The grains of the cross-section are not uniform. Given the differences in microstructures, the cross-

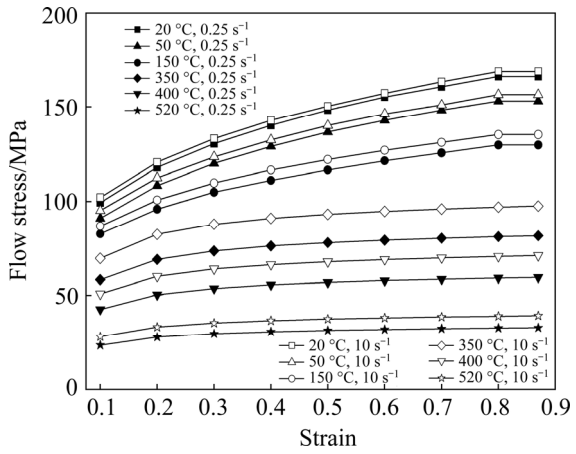

Fig. 4 Flow stress as function of strain, strain rate (0.25 and 10 s^{-1}) and temperature

section is divided into the welding, transition, and matrix zones. The detailed microstructures of the welding zone (denoted by *A* in Fig. 2(a)) are shown in Fig. 5. It can be seen that the weld seams gradually become refined and a portion of seam lines slowly disappear as the rotational speed increases from 6 to 11 r/min. Figure 6 shows that the transition zone (denoted by *B* in Fig. 2(a)) is characterized by large irregular-shaped grains with several hundred micrometers, which are caused by the abnormal growth of grains. The grain size of the transition zone shows a slight decreasing tendency with the increase of extrusion speed. Figure 7 exhibits the microstructures of the matrix zone (denoted by *C* in Fig. 2(a)). The average grain size of the matrix zone also shows a decrease from 147 to 103 μm as the rotational speed increases from 6 to 11 r/min.

4.2 Tensile properties and fracture surfaces

4.2.1 Mechanical properties

Figure 8 illustrates the mechanical properties of specimens under different rotational speeds. When the rotational speed increases from 6 to 11 r/min, the ultimate tensile strengths (UTS) and the elongations of specimens with 90°- and 45°-weld increase, thereby gradually approximating the corresponding matrix specimens. The experimental results show that the UTS ratios of the 90°- and 45°-weld specimens to those of the matrix specimens increase from 70.6% and 75.3% to 98.5% and 95.6%, respectively. While the elongation ratios of the 90°- and 45°-weld specimens to those of the matrix specimens increase from 35.4% and 41.1% to 77.7% and 81.5% respectively.

4.2.2 Fracture surfaces

Figure 9 shows the macro-fractographs of tensile specimens with a 90°-weld formed under different rotational speeds. All macroscopic fracture morphologies of specimens are composed of two

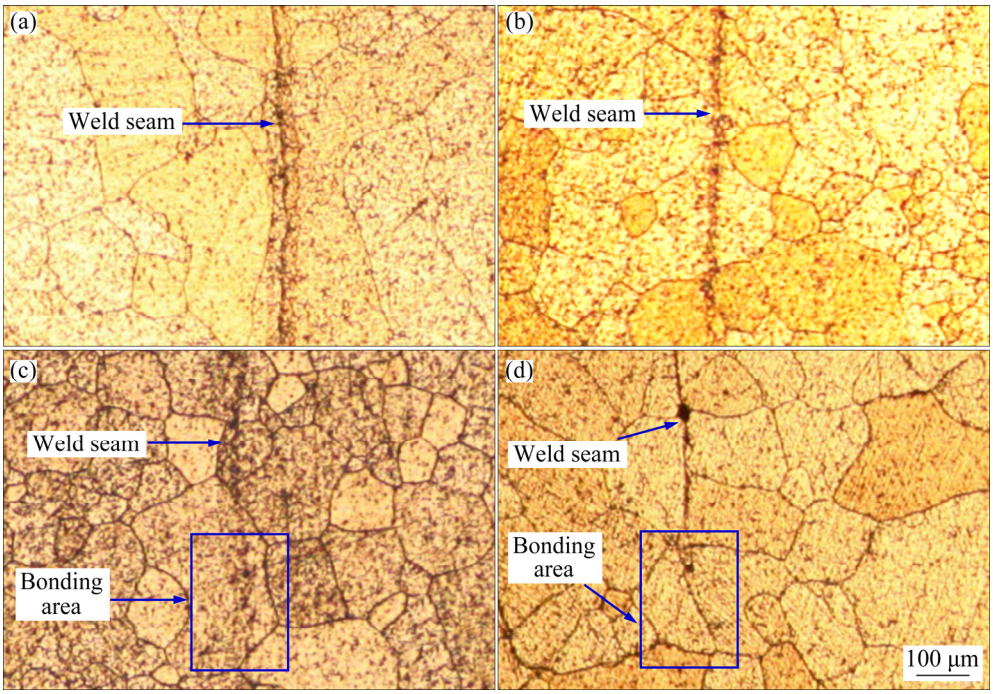

Fig. 5 Microstructures of weld seam *A* in Fig. 2(a) formed at different rotational speeds: (a) 6 r/min; (b) 7 r/min; (c) 9 r/min; (d) 11 r/min

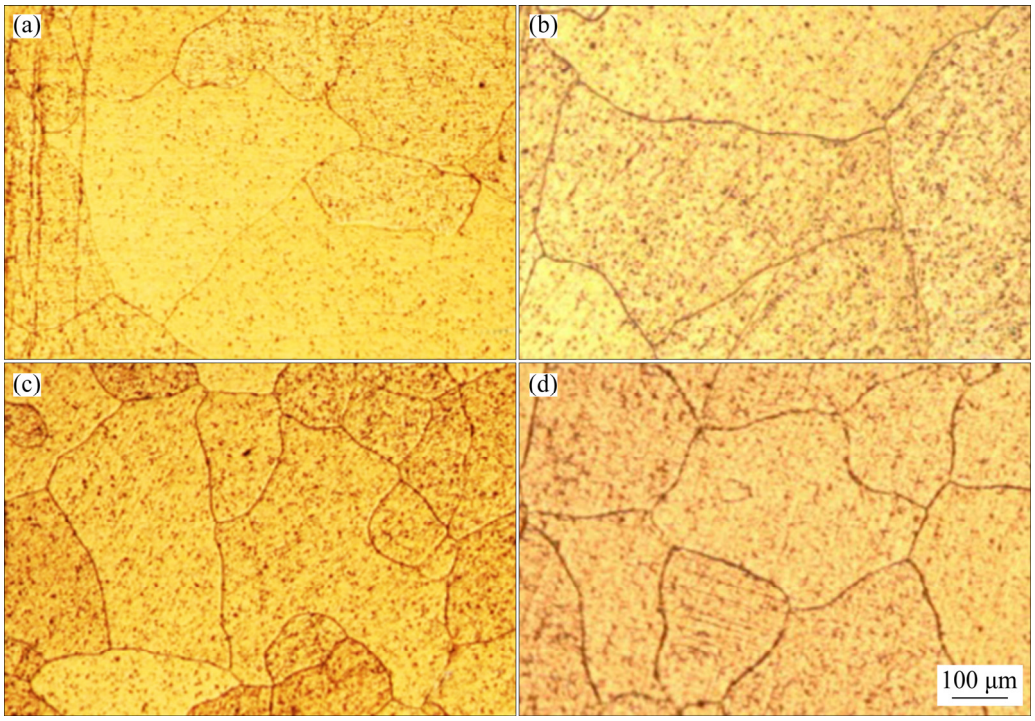

Fig. 6 Microstructures of transition zone *B* in Fig. 2(a) formed at different rotational speeds: (a) 6 r/min; (b) 7 r/min; (c) 9 r/min; (d) 11 r/min

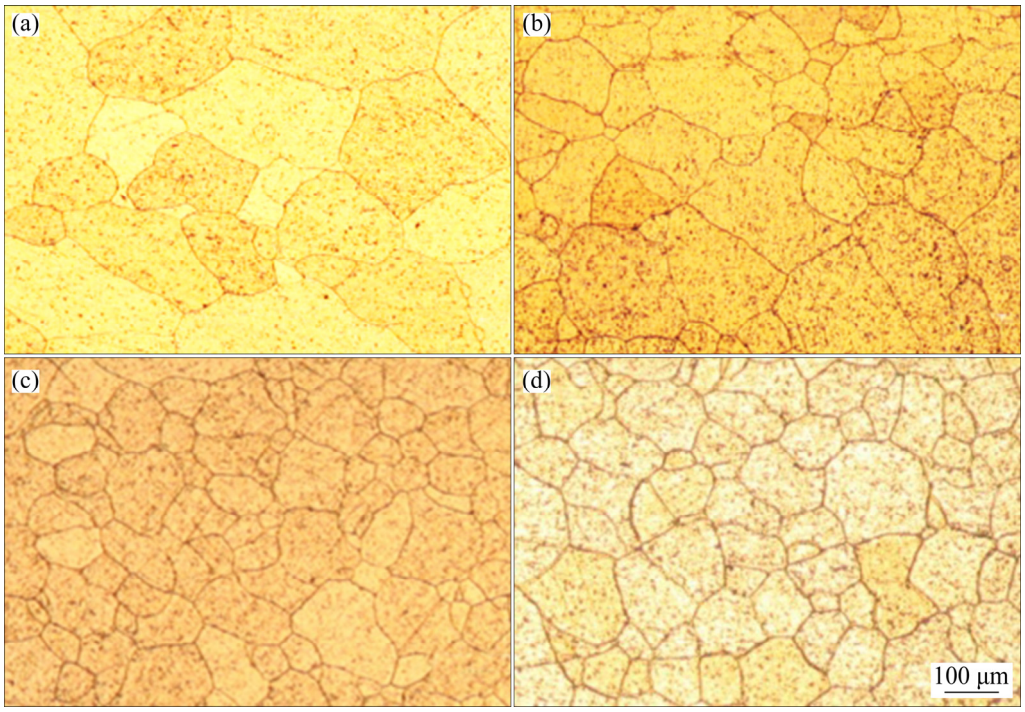

Fig. 7 Microstructures of matrix zone *C* in Fig. 2(a) formed at different rotational speeds: (a) 6 r/min; (b) 7 r/min; (c) 9 r/min; (d) 11 r/min

structures. One is the stripe structure located in the middle of the fracture surface, and the other is the dimple morphology, which is a typical plastic fracture characteristic. Stripe structures consist of fine dimples with a diameter of several microns and stripe-shaped protrusions under high magnification. The direction of the stripes corresponds to with the metal extrusion direction. Notably, the proportion

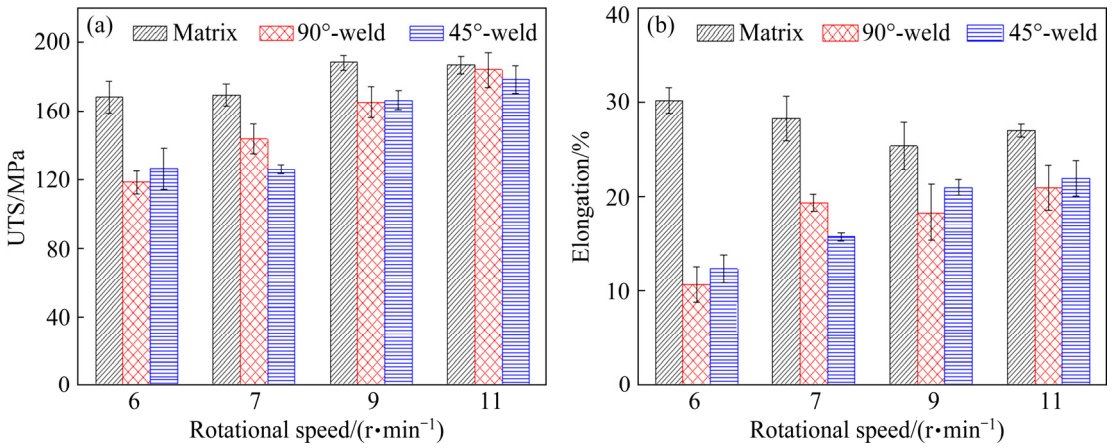

Fig. 8 UTS and elongation of product prepared at different rotational speeds: (a) UTS; (b) Elongation

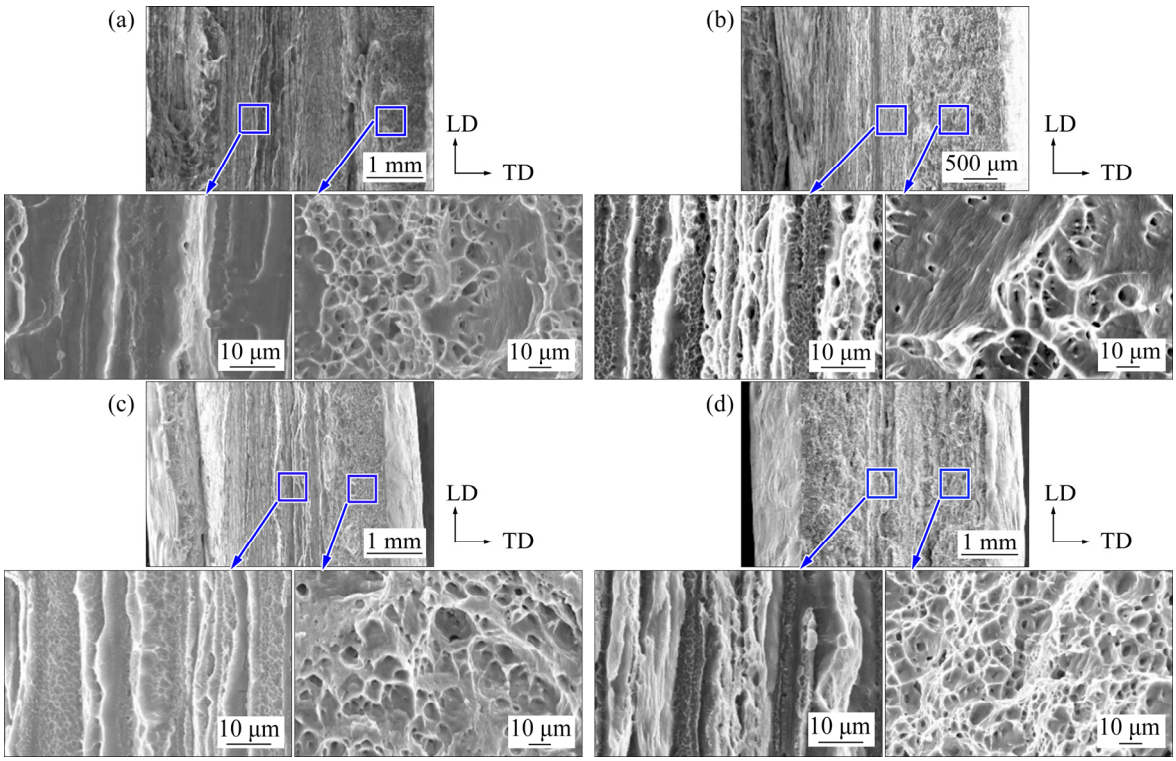

Fig. 9 Macro-fractographs of 90°-weld specimens formed at different rotational speeds: (a) 6 r/min; (b) 7 r/min; (c) 9 r/min; (d) 11 r/min

of the stripe morphology on the fracture surface gradually decreases as the rotational speed increases.

Figure 10 presents the stripe morphology distribution of the fracture surface along the thickness direction (TD) of specimens. Percentages of the width of the stripe morphology to the width of the specimen are 52%, 45%, 40%, and 15% at rotational speeds of 6, 7, 9, and 11 r/min, respectively. The stripe morphology represents the unbonded surface. The increase in extrusion speed evidently indicates that the proportion of the welding interface that fails to reach metallurgical bonding gradually decreases and the welding performance of products is improved gradually.

4.3 FEM simulation

The variation of extrusion speed will affect welding parameters and eventually influence the welding performance. The effects of extrusion speed on the welding parameters are discussed through FEM when the metal enters the stable

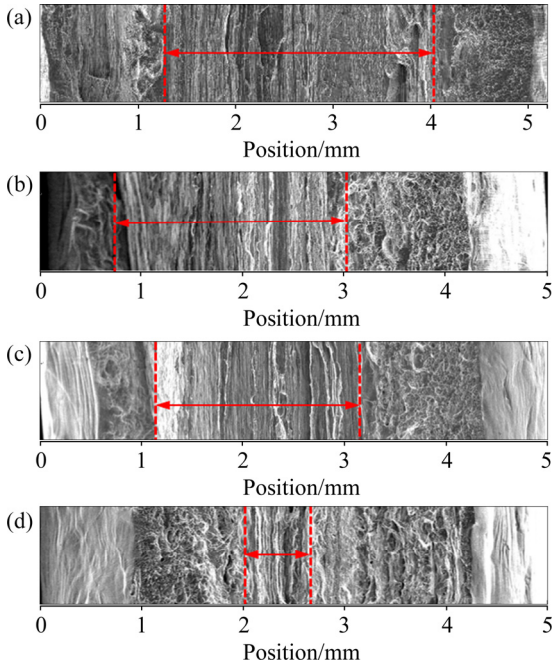

Fig. 10 Stripe morphologies of fracture along thickness direction of specimens prepared at different rotational speeds: (a) 6 r/min; (b) 7 r/min; (c) 9 r/min; (d) 11 r/min

deformation stage. Figure 11 shows the welding plane in the die cavity and characteristic points from the top to bottom along the welding path *A*–*B*. Starting point *A* is set at the top of the welding plane, while end point *B* is located at the die bearing. Data of temperature, effective stress, welding pressure, velocity and effective strain rate of characteristic points on the welding plane can be obtained through simulation, as shown in Figs. 12−16.

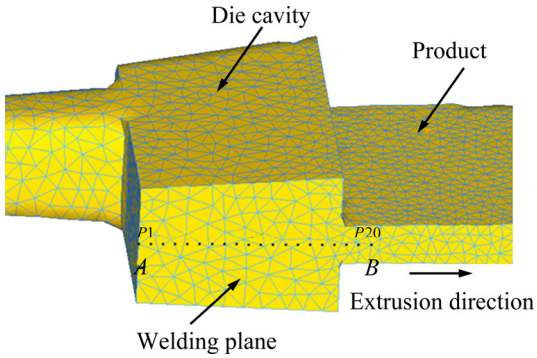

Fig. 11 Characteristic points along welding path

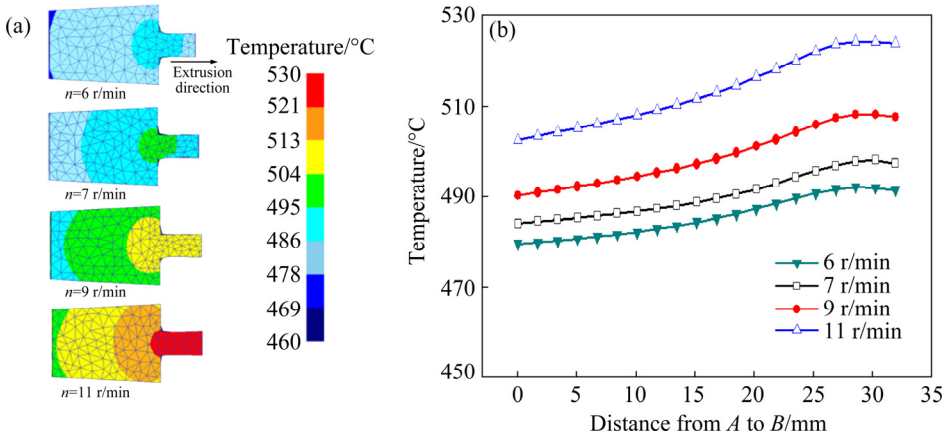

Fig. 12 Simulated temperature on welding plane at different rotational speeds: (a) In welded specimen; (b) Along welding path *A*–*B*

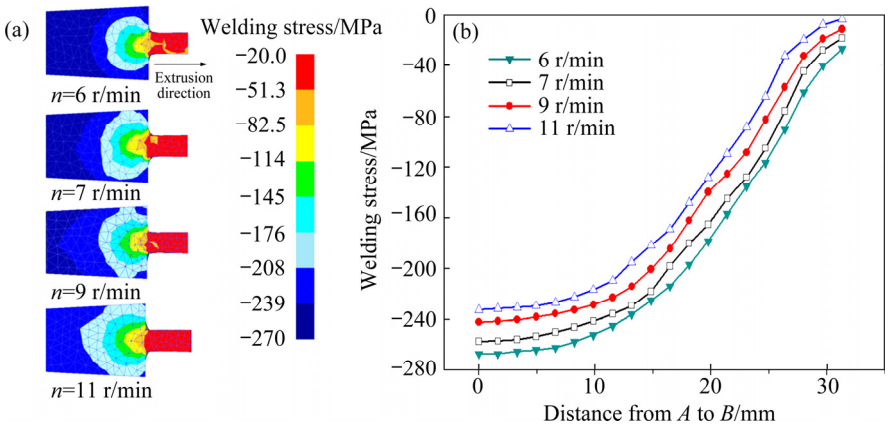

Fig. 13 Simulated welding stress on welding plane at different rotational speeds: (a) On welded plane; (b) Along welding path *A*–*B*

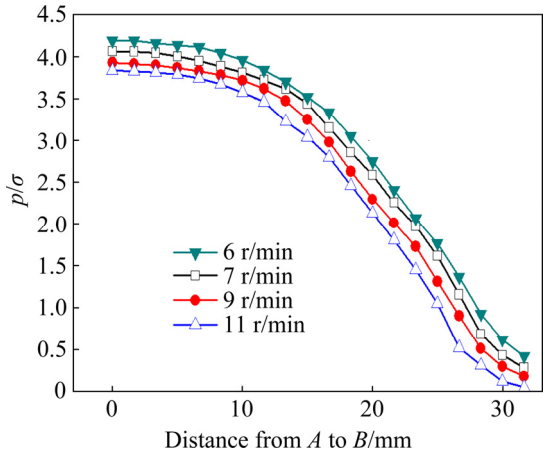

Fig. 14 Variation of ratios of welding stress to effective stress at different rotational speeds

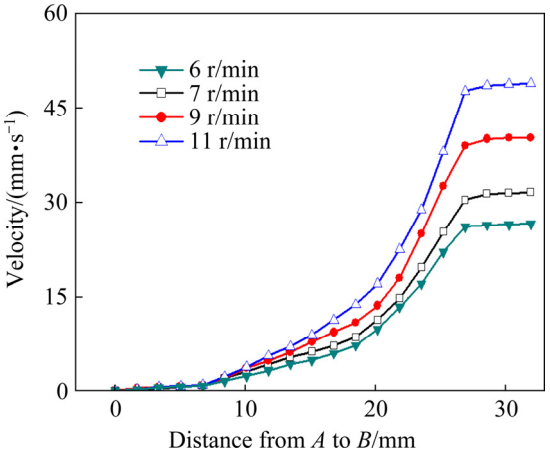

Fig. 15 Simulated velocities along welding path *A*–*B* at different rotational speeds

Figure 12 shows that the welding temperature increases along welding path *A*–*B*. The temperature reaches the maximum at the die orifice because of strong plastic deformation. The maximum values are 492, 498, 508, and 524 °C when rotational speeds are 6 to 7, 9, and 11 r/min, respectively. Corresponding temperatures at the outlet of the product in the experiment measured with an infrared thermometer are 502, 509, 524, and 538 °C, which have reached the solution temperature. The welding temperature rises approximately 30 °C when the rotational speed increases from 6 to 11 r/min.

Figure 13 presents the decreasing trend of the welding stress with increasing extrusion speed. The maximum welding stresses appear at the top of the die cavity. The maximum values are 267, 257, 242, and 232 MPa when rotational speeds are 6, 7, 9, and 11 r/min, respectively. The corresponding stresses on the abutment measured with the strain gauges are 685, 666, 659, and 632 MPa in the experiment. Thus, the stress in the die cavity and welding stress demonstrate the same declining trends with increasing rotational speed, thereby proving that the simulation results are reasonable. The simulation results show that the effective stress on the welding plane decreases with an increase in rotational speed, which is mainly caused by the increased temperature [10]. Figure 14 depicts the variation of the ratios of welding stress to effective stress (p/σ) at different rotational speeds. The distribution indicates that the p/σ ratio decreases along the welding path *A*–*B* and the maximum value appears at the top of the die cavity. The p/σ ratio decreases when extrusion wheel rotational speed increases. Figure 15 shows the simulated velocities along the welding path *A*–*B* under different rotational speeds. The dead metal zone observed within 8 mm from the top (point *A*) of the

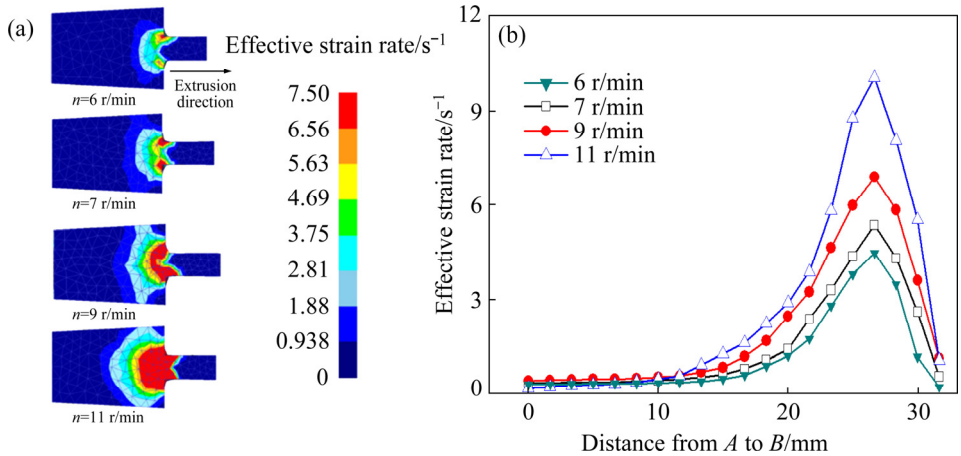

Fig. 16 Simulated effective strain rate on welding plane at different rotational speeds: (a) On welding plane; (b) Along welding path *A*–*B*

cavity is caused by the extension and welding formation of double billets in the die cavity. The metal in the dead zone minimally contributes to the welding. Therefore, the effective welding path is considered in the analysis of p/σ and the maximum values of p/σ in the effective welding path are 4.0, 3.9, 3.8, and 3.7 at rotational speeds of 6, 7, 9, and 11 r/min, respectively.

Figure 16 shows the simulation results of the effective strain rate on the welding plane at different rotational speeds. The distribution indicates that the effective strain rate increases initially and then decreases along the welding path *A*–*B*, and the maximum value appears at the die orifice. The effective strain rate clearly increases when the rotational speed increases from 6 to 11 r/min, with the maximum values of 4.5, 5.4, 6.9, and 10.1 s^{-1}, at rotational speeds of 6, 7, 9, and 11 r/min, respectively.

5 Discussion

The metal welding is significantly affected by the oxide on the outer surface of the billet with serious welding condition in the case of the continuous extrusion process of double billets without the division stage compared with the welding process in conventional extrusion with porthole die. The metal welding in continuous extrusion deformation takes place in the following process. The welding interface comes into contact and micro-voids are formed under a certain pressure first. These micro-voids must close through plastic deformation and atomic diffusion under certain pressure, effective strain, and temperature [11]. Metallurgical bonding can be formed between virgin metals only when the oxide on the outer surface of the billet reaches a sufficient broken degree after the void closes in this process [12].

The ratio of the welding stress to effective stress is calculated to analyze the influence of the extrusion speed on welding. NAKASAKI et al [13] indicated that the increased stress ratio contributes to the closure of micro-voids at the weld seam. The increase in extrusion speed that decreases the ratio of welding stress to effective stress is not conducive to the closure of micro-voids at the weld seam. The maximum p/σ value in the effective welding path is only reduced by 7.5% when the rotational speed increases from 6 to 11 r/min, thereby indicating the slight adverse effect on welding.

OOSTERKAMP and OOSTERKAMP [14] and COOPER and ALLWOOD [15] reported that high temperature is conducive to the formation of metallurgical bonding due to the diffusion of atoms in the welding process. The present study showed that the temperature of the welding plane gradually increases approximately 30 °C as the rotational speed increases from 6 to 11 r/min. Therefore, the increased temperature accelerates the formation of metallurgical bonding.

The contribution of effective strain rate to welding has gained increasing attention in recent years. The strain rate influences the degree of the contaminant breakage and virgin material exposure [16,17]. The current study demonstrated that the maximum effective strain rate increases approximately twice when the rotational speed increases from 6 to 11 r/min. The degree of oxide breakage on the welding surface increases due to the evident increase in the effective strain rate with increasing rotational speed. Accordingly, additional virgin metals start to contact and form metallurgical welding and the proportion of the welding interface that fails to reach metallurgical bonding gradually reduces. Given that oxide particles on the weld seam layer exhibit poor corrosion resistance, the microstructure observation indicated that weld seam lines gradually become refined and a portion of these lines gradually disappear when the rotational speed increases from 6 to 11 r/min. Accordingly, the tensile strength and the elongation of the weld specimen increase with increasing rotational speed. The increased effective strain rate plays an important role in the variation of the welding performance as the rotational speed increases.

Grain sizes of transition and matrix zones decrease with increasing rotational speed. Dynamic recrystallization of metal in continuous extrusion occurs before it enters the cavity due to the severe deformation of the billet in the bending zone [18,19]. On one hand, increasing the extrusion speed can lead to the increase of strain rate. Moreover, the high strain rate inhibits grain growth [20,21]. Thus, the increased deformation speed leads to a decrease in grain sizes of transition and matrix zones. On the other hand, growth time of recrystallized grains in the die cavity that decreases with increasing speed is beneficial to the refinement of grains.

6 Conclusions

(1) When the rotational speed of the extrusion wheel increases from 6 to 11 r/min, the welding temperature increases approximately 30 °C, the maximum p/σ value in the effective welding path decreases by 7.5%, and the maximum equivalent strain rate increases up to more than twice.

(2) Weld seam lines gradually become refined and a portion of these seam lines slowly disappear with the increase of extrusion speed. The proportion of the welding interface that fails to reach metallurgical bonding gradually reduces. The tensile strength and the elongation of the weld specimen increase evidently.

(3) The degree of oxide breakage on the welding surface increases due to the evident increase in effective strain rate with increasing extrusion speed. The high temperature induced by increasing extrusion speed accelerates the formation of metallurgical bonding. Therefore, the increase of effective strain rate and temperature contributes to the metallurgical bonding of welding interface as the extrusion speed increases.

Acknowledgments

The authors are grateful for the financial supports from the National Natural Science Foundation of China (Nos. 51705062, 51675074), and the Department of Education Fund Item of Liaoning Province, China (No. JDL 2019021).

References

[1] DENG Yun-lai, ZHANG Xin-ming. Development of aluminium and aluminium alloy [J]. The Chinese Journal of Nonferrous Metals, 2019, 29(9): 2115−2141. (in Chinese)

[2] DEN-BAKKER A J, WERKHOVEN R J, SILLEKENS W H, KATGERMAN L. The origin of weld seam defects related to metal flow in the hot extrusion of aluminium alloys EN AW-6060 and EN AW-6082 [J]. Journal of Materials Processing Technology, 2014, 214: 2349−2358.

[3] YI Jie, WANG Zhen-hu, LIU Zhi-wen, ZHANG Jian-ming, HE Xin. FE analysis of extrusion defect and optimization of metal flow in porthole die for complex hollow aluminium profile [J]. Transactions of Nonferrous Metals Society of China, 2018, 28(10): 2094−2101.

[4] ZHANG Xin-ming, FENG Di, SHI Xing-kuan, LIU Sheng-dan. Oxide distribution and microstructure in welding zones from porthole die extrusion [J]. Transactions of Nonferrous Metals Society of China, 2013, 23(3): 765−772.

[5] LIU Zhi-wen, LI Luo-xing, YI Jie, LI Shi-kang, WANG Guan. Influence of extrusion speed on the seam weld quality in the porthole die extrusion of AZ31 magnesium alloy tube [J]. International Journal of Advanced Manufacturing Technology, 2017, 92: 1039−1052.

[6] LIU G, ZHOU J, DUSZCZYK J. FE analysis of metal flow and weld seam formation in a porthole die during the extrusion of a magnesium alloy into a square tube and the effect of ram speed on weld strength [J]. Journal of Materials Processing Technology, 2008, 200: 185−198.

[7] YU Jun-quan, ZHAO Guo-qun, CUI Wei-chao, ZHANG Cun-sheng, CHEN Liang. Microstructural evolution and mechanical properties of welding seams in aluminum alloy profiles extruded by a porthole die under different billet heating temperatures and extrusion speeds [J]. Journal of Materials Processing Technology, 2017, 247: 214−222.

[8] LI Shi-kang, LI Luo-xing, LIU Zhi-wen, WANG Guan. Effect of extrusion speed on weld strength of 6063 square tube [J]. The Chinese Journal of Nonferrous Metals, 2017, 27(9): 1775−1784. (in Chinese)

[9] BAI Sheng-wen, FANG Gang, ZHOU Jie. Integrated physical and numerical simulations of weld seam formation during extrusion of magnesium alloy [J]. Journal of Materials Processing Technology, 2019, 266: 82−95.

[10] QUAN G Z, KU T W, SONG W J, KANG B S. The workability evaluation of wrought AZ80 magnesium alloy in hot compression [J]. Materials and Design, 2011, 32: 2462−2468.

[11] TANG Ding, ZHANG Qing-qing, FANG Wen-li, LI Da-yong, PENG Ying-hong. Modeling of the extrusion seam welding based on the void evolution [J]. Journal of Mechanical Engineering, 2014, 50(22): 34−41.

[12] COOPER D R, ALLWOOD J M. The influence of deformation conditions in solid-state aluminium welding processes on the resulting weld strength [J]. Journal of Materials Processing Technology, 2014, 214: 2576−2592.

[13] NAKASAKI M, TAKASU I, UTSUNOMIYA H. Application of hydrostatic integration parameter for free-forging and rolling [J]. Journal of Materials Processing Technology, 2006, 177: 521−524.

[14] OOSTERKAMP A, OOSTERKAMP L D. “Kissing bond” phenomena in solid-state welds of aluminum alloys [J]. Welding Journal, 2004, 83: 225–231.

[15] COOPER D R, ALLWOOD J M. Influence of diffusion mechanisms in aluminium solid-state welding processes [J]. Procedia Engineering, 2014, 81: 2147−2152.

[16] YU Jun-quan, ZHAO Guo-qun, CHEN Liang. Analysis of longitudinal weld seam defects and investigation of solid-state bonding criteria in porthole die extrusion process of aluminum alloy profiles [J]. Journal of Materials Processing Technology, 2016, 237: 31−47.

[17] NAKASAKI M, TAKASU I, UTSUNOMIYA H. Application of hydrostatic integration parameter for free-forging and rolling [J]. Journal of Materials Processing Technology, 2006, 177: 521−524.

[18] ZHAO Ying, SONG Bao-yun, PEI Jiu-yang, JIA Chun-bo, LI Bing, GUO Lin-lin. Effect of deformation speed on the microstructure and mechanical properties of AA6063 during continuous extrusion process [J]. Journal of Materials

Processing Technology, 2013, 213: 1855−1863.
[19] HE Y L, GAO F, SONG B Y, FU R, WU G M, LI J, JIANG L. Grain refinement of magnesium alloy by conform: A continuous severe plastic deformation route [J]. Materials Science Form, 2012, 706−709: 1781−1786.
[20] FATEMI-VARZANEH S M, ZAREI-HANZAKI A, BELADI H. Dynamic recrystallization in AZ31 magnesium alloy [J]. Materials Science and Engineering A, 2007, 456(1): 52−57.
[21] LI Shi-kang, LI Luo-xing, HE Hong, LIU Zhi-wen, WANG Guan, ZHANG Long. Influence of dynamic recrystallization on microstructure and mechanical properties of welding zone in Al−Mg−Si aluminum profile during porthole die extrusion [J]. Transactions of Nonferrous Metals Society of China, 2019, 29(9): 1803−1815.

挤压速度对双坯料连续挤压 6063 铝合金焊合性能的影响

赵 颖，裴久杨，郭丽丽，运新兵，马怀超

大连交通大学 连续挤压教育部工程研究中心，大连 116028

摘 要：在双坯料连续挤压过程中，由于两根坯料汇合而形成挤压焊缝。通过显微组织观察、拉伸试验、扫描电镜研究挤压轮转速对 6063 铝合金焊缝显微组织形貌和性能的影响，并通过有限元仿真分析焊合参数。结果表明，在连续挤压过程中，坯料外表面的氧化物对金属焊合有显著影响，随着挤压速度的增加，等效应变速率明显增加，造成焊合面上的氧化物的破碎程度增加。提高挤压速度所引起的高温加速焊合界面形成冶金结合，部分焊合线逐渐消失，焊合界面上未达到冶金结合的焊缝所占比例逐渐降低。随着挤压速度的增加，焊缝试样的抗拉强度和伸长率均增大。

关键词：连续挤压；6063 铝合金；挤压速度；焊合性能

(Edited by Wei-ping CHEN)